forests

MDPI

Article

Daily Actual Evapotranspiration Estimation in a Mediterranean Ecosystem from Landsat Observations Using SEBAL Approach

Hassan Awada [1,*], Simone Di Prima [1], Costantino Sirca [1,2], Filippo Giadrossich [1], Serena Marras [1,2], Donatella Spano [1,2] and Mario Pirastru [1]

[1] Department of Agricultural Sciences, University of Sassari, Viale Italia 39, 07100 Sassari, Italy; sdiprima@uniss.it (S.D.P.); cosirca@uniss.it (C.S.); fgiadrossich@uniss.it (F.G.); serenam@uniss.it (S.M.); spano@uniss.it (D.S.); mpirastru@uniss.it (M.P.)

[2] Euro-Mediterranean Centre on Climate Change (CMCC) Foundation, Via de Nicola 9, 07100 Sassari, Italy

* Correspondence: hassan_awada1987@live.com

Abstract: Quantifying actual evapotranspiration (ET_a) over natural vegetation is crucial in evaluating the water status of ecosystems and the water-use patterns in local or regional hydrological basins. Remote sensing-based surface energy balance models have been used extensively for estimating ET_a in agro-environments; however, the application of these models to natural ecosystems is still limited. The surface energy balance algorithm for land (SEBAL) physical-based surface energy balance model was applied to estimate the actual evapotranspiration over a heterogeneous coverage of Mediterranean maquis in a natural reserve in Sardinia, Italy. The model was applied on 19 Landsat 5 and 8 images from 2009 to 2014, and the results were compared to the data of a micrometeorological station with eddy covariance flux measurements. Comparing the SEBAL-based evaporative fraction (Λ_S) to the corresponding tower-derived evaporative fractions (Λ_T) showed good flux estimations in the Landsat overpass time (Coefficient of determination $R^2 = 0.77$, root mean square error RMSE = 0.05 and mean absolute error MAE = 0.076). Three methods were evaluated for upscaling instantaneous latent heat flux (λE) to daily actual evapotranspiration ($ET_{a,D}$). The upscaling methods use the evaporative fraction (Λ), the reference evapotranspiration fraction (EF_r) and the ratio of daily to instantaneous incoming shortwave radiation (Rs_{24}/Rs_i) as upscaling factors under the hypothesis of diurnal self-preservation. A preliminary analysis performed using only in-situ measured data demonstrated that the three factors were relatively self-preserved during the daytime, and can yield good $ET_{a,D}$ estimations, particularly when obtained at near the Landsat scene acquisition time (≈10:00 UTC). The upscaling factors obtained from SEBAL retrieved instantaneous fluxes, and some ancillary measured meteorological data were used to upscale SEBAL-estimated instantaneous actual λ to daily ET. The Λ EFr and Rs_{24}/Rs_i methods on average overestimated the measured $ET_{a,D}$ by nearly 20, 61 and 18%, respectively. The performance of the Λ and Rs_{24}/Rs_i methods was considered satisfactory, bearing in mind the high variable ground cover and the inherent variability of the biome composition, which cannot be properly represented in the Landsat moderate spatial resolution. In this study, we tested the potential of the SEBAL model application in a complex natural ecosystem. This modeling approach will be used to represent the spatial dynamics of ET, which will be integrated into further environmental and hydrological applications.

Keywords: Mediterranean maquis; remote sensing; SEBAL; actual evapotranspiration; eddy covariance; evaporative fraction; upscaling methods

Citation: Awada, H.; Di Prima, S.; Sirca, C.; Giadrossich, F.; Marras, S.; Spano, D.; Pirastru, M. Daily Actual Evapotranspiration Estimation in a Mediterranean Ecosystem from Landsat Observations Using SEBAL Approach. *Forests* **2021**, *12*, 189. https://doi.org/10.3390/f12020189

Academic Editor: Manuel Esteban Lucas-Borja

Received: 8 January 2021

Accepted: 3 February 2021

Published: 7 February 2021

1. Introduction

Understanding eco-hydrological processes is critical for evaluating ecosystem resilience and vulnerability [1]. Evapotranspiration (ET) is one of the most critical components

of the land-surface water and energy budget, particularly in arid and semi-arid Mediterranean environments. Chen et al. [2] demonstrated the importance of biotic hydrological processes, particularly the interactions between terrestrial vegetation and hydrology (i.e., canopy interception and ET). The ET variability is a key indicator of ecosystem complexity. Quantifying the spatial and temporal dynamics of ET can help in the assessment of ecosystem sustainability and climate variability. Vincente-Serrano et al. [3] proposed the use of ET and precipitation data as a multi-scalar drought index in the context of global warming. Spano et al. [4] highlighted that, in forest ecosystems, managers need a practical method for continuous, historical and near real-time ET estimation to guide forest management.

Several ground-based ET measurement techniques are available and are widely used, including micrometeorological techniques such as eddy covariance [5–7], scintillometry [8,9], the Bowen ratio [10,11] and surface renewal [12,13]. Other ground-based methods measure ET directly by soil-weighing lysimeters [14–16], or estimate it by soil water balancing techniques [17,18]. Some methods measure plant transpiration via sap flow [19,20]. Even though field-based methods provide accurate ET measurements, these methods are labor- and cost-intensive [21,22], and require skilled operational staff. Moreover, these measurements are representative of a local spatial scale, from single plant to footprint area. Interpolating or extrapolating such measurements over larger spatial scales can misrepresent the ET variability, particularly for natural environments, where eco-hydrologic studies revealed considerable spatial and temporal variability in plant–water interactions due to microclimatic, land and vegetation heterogeneity [23–25]. In this context, there is a need for different methodologies that allow the estimation of ET of natural vegetation over a broader scale.

Knowing that the ET process is governed by the energy exchanges in the soil–plant-atmosphere (SPA) system and is limited by the available energy at the land surface, ET can be retrieved by applying the energy conservation principle to the land surface energy balance (SEB). Several models are used to provide an instantaneous estimation of actual ET as a residual term of the land surface energy balance [26–35]. Such models apply the SEB approach to available free or low-cost earth observation data [21,36]. Satellite-based SEB models have been validated on agricultural land in various parts of the world [26,28,37–39]. The SEB approach for modeling ET spatial distribution was extensively used in irrigation management [26,40–42], water accounting [43], assessing irrigation system performance [36,44,45], agricultural water productivity [46,47], groundwater management [48–50], and hydrological modeling [51–54]. Although the remotely sensed surface energy balance ET approach is widely accepted and used, and despite its ability to provide spatially distributed ET estimation, most of the applications were aimed at hydrological studies and water management in agriculture. According to the author's knowledge, a gap still exists in the application of this approach to natural ecosystems.

Mediterranean forest ecosystems provide multiple environmental and socio-economic goods and services. The Mediterranean maquis is a formation of a complex multi-strata structure that represents a dynamic inter-equilibrium, including small trees, tall bushes, dwarf bushes, grasses and microorganisms [55], adapted and resistant to semi-arid condition. In the last few decades Mediterranean forests have been subjected to numerous threats, such as forest fires, over-exploitation, deforestation, and degradation, which are accentuated in the context of climate and land-use changes [56]. Pirastru et al. [57] demonstrated the effects of Mediterranean maquis clearing on soil properties and near-surface hydrology. Folton et al. [58] demonstrated the changes in the hydrological response of a Mediterranean sub-catchment as a result of changes in land physical condition due to wildfire, and Niedda and Pirastru [59] showed the severe effects of land-use and climate changes on the water resources availability in a small Mediterranean catchment in northern Sardinia, Italy.

In this paper, we applied the surface energy balance algorithm for land (SEBAL) model [27,60,61] using Landsat moderate-resolution imagery to estimate ET over a natural

Mediterranean ecosystem. SEBAL is a single-source model, and it does not differentiate between components within a single pixel (e.g., soil and vegetation) [62,63]. The model requires surface radiometric temperature derived from thermal infrared radiation on a cloud-free image scene [64,65]. In addition to remote sensing (RS) data, SEBAL relies on a few ground-based ancillary meteorological data [26,60]. The model has been previously and extensively validated under a range of environmental conditions in agricultural land [37,61]. However, there is a need to further verify its potential in natural environments.

SEBAL initially retrieves the net radiation, Rn, soil heat flux at the surface, G_0, and sensible heat flux, H, at the satellite overpass time, then estimates latent heat flux, λE, as the residual term of the energy budget. The λE represents the energy attributed to the instantaneous actual evapotranspiration. The SEBAL model uses the evaporative fraction (i.e., the ratio of the latent heat flux to the available energy, $Rn–G_0$) to upscale instantaneous estimations of the actual evapotranspiration at the satellite overpass time to daily values [28,36], and operates under the hypothesis of diurnal self-preservation of the evaporative fraction [66–69]. Alternative upscaling methods that also rely on daytime preservation use the reference crop evapotranspiration [70,71] and the incoming shortwave radiation [72,73] as upscaling parameters.

The general objective of this paper is to evaluate the potential of the SEBAL model combined with Landsat 5 and 8 images in estimating actual ET over a natural ecosystem typical to the Mediterranean coasts. The study is performed over a Mediterranean maquis ecosystem in northwest Sardinia, Italy.

Specifically, this study is carried out with the following objectives:

i. testing the diurnal self-preservation hypothesis and different ET upscaling methods based on in-situ flux measurements;
ii. evaluating the SEBAL model's performance in estimating instantaneous surface energy fluxes over Mediterranean maquis using the evaporative fraction;
iii. evaluating the upscaling methods for retrieving daily actual ET values from instantaneous SEBAL evapotranspiration estimates of Mediterranean maquis.

2. Materials and Methods

2.1. Study Area

The study site is located inside a natural reserve called "Le Prigionette", Northwest Sardinia, Italy. The climate is Mediterranean, semi-arid with a warm summer, mild winter, and a high water deficit from May through September. The mean annual temperature is 15.9 °C, the minimum and maximum temperature are 7.0 °C and 28.6 °C, respectively. Precipitation is mainly concentrated from autumn to spring and the annual mean is 588 mm. The soil is 0.3–0.4 m deep Lithic Xerorthent. The ecosystem is a typical coastal Mediterranean maquis (schlerophyll species) mainly consisting of juniper (*Juniperus phoenicea* L.), lentisk (*Pistacia lentiscus* L.), tree phyllirea (*Phyllirea angustifolia* L.), and dwarf fan palm (*Chamaerops humilis* L.). These species form sparsely vegetated shrub land, in which juniper and lentisk cover 53% and 22% of the vegetated surface, respectively, and they are aggregated into variable-sized patches. Tree phillyrea and palm are found only as isolated elements inside the main patches. Other species present in the experimental site are rosemary (*Rosmarinus officinalis* L.), *Genista corsica* (Loisel) DC., *Daphne gnidium* L., *Smilax aspera* L., *Euphorbia characias* L., *Helichrysum microphyllum* DC., *Asphodelus microcarpus* Salzm., and *Ferula communis* L. The vegetation is a secondary succession following a fire event in 1963 and agricultural abandonment in 1970. The mean vegetation height ranges between 0.93 and 1.43 m. Ground cover varies between 42% and 91%.

2.2. Micrometeorological and Eddy Covariance Measurements

Eddy Covariance (EC) data were collected by the micro-meteorological station (IT-Noe), installed in the study area as part of the CARBOEUROPE flux monitoring network [74]. The monitoring site is located at the Le Prigionette natural reserve (lat: 40.61, lon:

8.15, 25 m of elevation above sea level) (Figure 1). The IT-Noe station consists of an EC system with a sonic anemometer (CSAT3, Campbell Scientific, Logan, UT, USA) and an open path gas analyzer (LiCOR 7500, Lincoln, NE, USA), placed within the maquis at 3.5 m above the ground for measuring λE and H. The station also measures G_0 by thermocouples and 4 heat flux plates (HFP01SC, Hukseflux, Delft, NL), installed at a depth of 0.08 m in the soil. The station also acquires downward and upward short and long wave radiation, air temperature, air humidity, precipitation, wind speed, and surface pressure at 2 m above the ground. EC data were processed using the software EOLO [4] that provides sensible and latent heat turbulent fluxes, soil heat flux, and momentum at a half-hour time step. Due to quality check flags and other causes (i.e., technical problems due to instruments and power supply), the EC system was able to collect, on average, about 80% of the data. Gaps were filled using the online tool available at: https://www.bgc-jena.mpg.de/~MDIwork/eddyproc/ (accessed on the 20 June 2020).

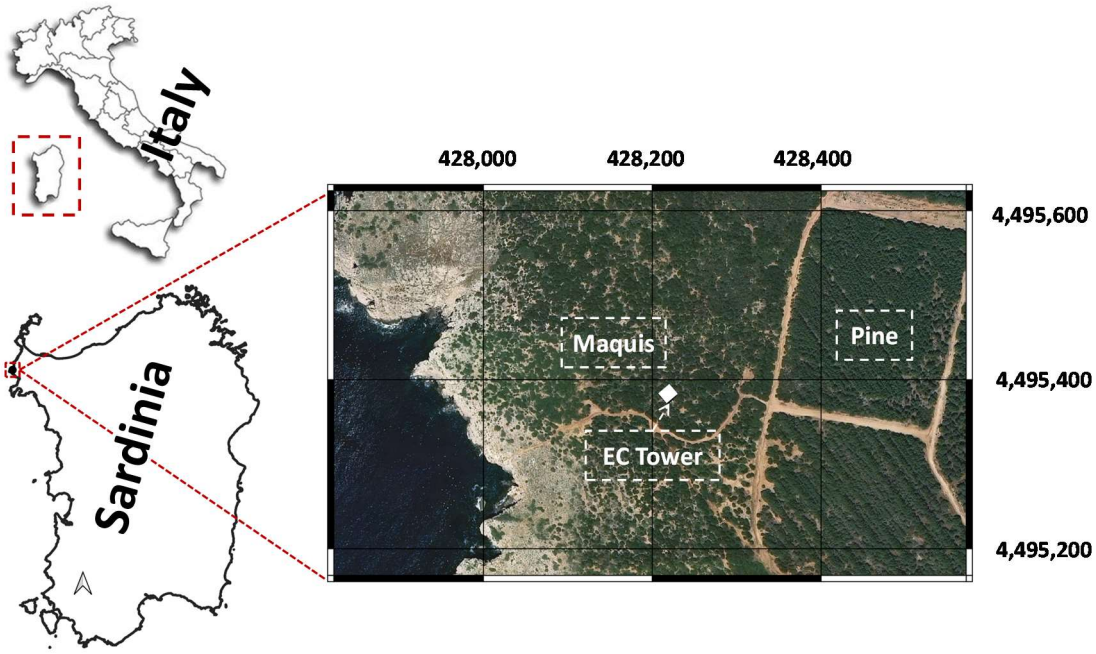

Figure 1. Geographic location of the micro-meteorological IT-Noe station in the Le Prigionette natural reserve, Italy. Coordinates EPSG:32632 (WGS 84/UTM zone 32N). The white square indicates the position of the eddy covariance tower.

Data from the IT-Noe station were obtained for the days that correspond to the selected Landsat satellite acquisitions (Table 1). Several studies have reported imbalances in the EC-measured SEB components [75–77]. Considering that RS surface energy balance modeling approaches estimate the instantaneous ET under the assumption of the surface energy budget closure, the measured data were corrected by forcing the energy closure using the Bowen ratio. Data quality was evaluated by the energy balance closure (C_R) representing the ratio of available energy to the turbulent flux components [75]. As suggested by Prueger et al. [78], C_R was assessed for Rn greater than 100 W m^{-2}:

$$C_R = \frac{H + \lambda ET}{Rn - G_0} \quad (1)$$

Wilson et al. [75] reported a typical energy budget closure error of 20%. Allen et al. [64] considered that measurements with ±15% energy budget closure error are reliable. Here the energy budget closure was deemed to be satisfactory when $C_R > 0.85$ [75,78]. However, knowing that the SEBAL model is based on energy balance closure and it is more reasonable to compare its results with the closure corrected ground-based data, force closure was applied to all data. The energy budget closure was forced by attributing

available energy Rn–G_0 to H and λET with the preservation of the Bowen ratio (β), defined as H/λET [78], as follows:

$$\lambda Ec = \frac{(Rn - G_0)}{(1 + \beta)} \quad (2)$$

$$Hc = \beta \frac{(Rn - G_0)}{(1 + \beta)} \quad (3)$$

where λET_c and H_c are the corrected values of the latent heat flux and of the sensible heat flux, respectively.

2.3. Landsat Satellites Datasets and Processing

A set of 14 Landsat 5 Thematic Mapper (TM) (paths 193 and 194, Row 32) images, and 5 Landsat 8 Operational Land Imager (*OLI*) and Thermal Infrared Sensor (TIRS) images were selected for the years from 2009 to 2014 (Table 1). The image selection was driven by both the presence of scene clear-sky acquisitions and good-quality EC tower data. Landsat images and metadata were obtained from the United States Geological Survey (USGS) Earth Explorer (https://earthexplorer.usgs.gov/), last accessed on the 10th of June 2020, and the *USGS Global Visualization Viewer* (GloVis) (https://glovis.usgs.gov/), last accessed on the 10th of June, 2020. We processed the surface reflectance from visible and infrared bands (near-infrared, mid-infrared and short-wave-infrared) (TM bands 1–5 and 7 and OLI bands 2–7) obtained at 30 m spatial resolution and Landsat thermal bands (TM 6th band and TIRS 10th band). The thermal infrared (TIR) bands were acquired at 120 m and 100 m spatial resolution for TM and TIRS, respectively. TIR data were resampled by the data providers using the cubic convolution method to a 30 m pixel size to match the multispectral bands. Landsat TM and OLI image subsets (cloud-free over study area) were created for the area of interest. Subset images were calibrated for atmospheric scattering and absorption by the "Second Simulation of a Satellite Signal in the Solar Spectrum code" (6S code) [79].

Table 1. Selected Landsat 5 (LS5) and Landsat 8 (LS8) images.

Image	Acquisition Day (dd/mm/yyyy)	DOY	Platform	Acquisition Time (Scene Center) (hh:mm UTC)	Pass	Row	Cloud Cover (%)
1	8/3/2009	67	LS5	9:52	193	32	0
2	11/5/2009	131	LS5	9:53	193	32	2
3	19/6/2009	170	LS5	10:00	194	32	0
4	21/7/2009	202	LS5	10:01	194	32	0
5	30/7/2009	211	LS5	9:55	193	32	0
6	6/8/2009	218	LS5	10:01	194	32	0
7	15/8/2009	227	LS5	9:55	193	32	0
8	22/8/2009	234	LS5	10:01	194	32	0
9	31/8/2009	243	LS5	9:55	193	32	4
10	7/9/2009	250	LS5	10:01	194	32	0
11	2/10/2009	275	LS5	9:56	193	32	14
12	28/4/2010	118	LS5	9:56	193	32	7
13	17/7/2010	198	LS5	9:56	193	32	0
14	6/11/2010	310	LS5	9:55	193	32	1
15	10/8/2013	222	LS8	10:07	193	32	6
16	29/10/2013	302	LS8	10:07	193	32	10
17	10/6/2014	161	LS8	10:05	193	32	1
18	28/7/2014	209	LS8	10:05	193	32	2
19	14/9/2014	257	LS8	10:06	193	32	8

2.4. The Surface Energy Balance Algorithm for Land (SEBAL) Model

The SEBAL algorithm is implemented in the ERDAS software Model Maker. SEBAL simulates the radiative and turbulent fluxes within an image pixel without differentiating between soil and vegetation (single-source approach). The SEBAL process flowchart is shown in Figure 2. The Landsat images, accompanied by a 10 m digital elevation model (DEM) (http://www.sardegnageoportale.it/) last accessed on the 15 June 2020 and half-hourly meteorological inputs, were used to produce the SEBAL data layers (i.e., land surface temperature, surface albedo, normalized difference vegetation index, and surface emissivity). SEBAL retrieves Rn, G_0 and H and estimates λE as a residue of the energy budget.

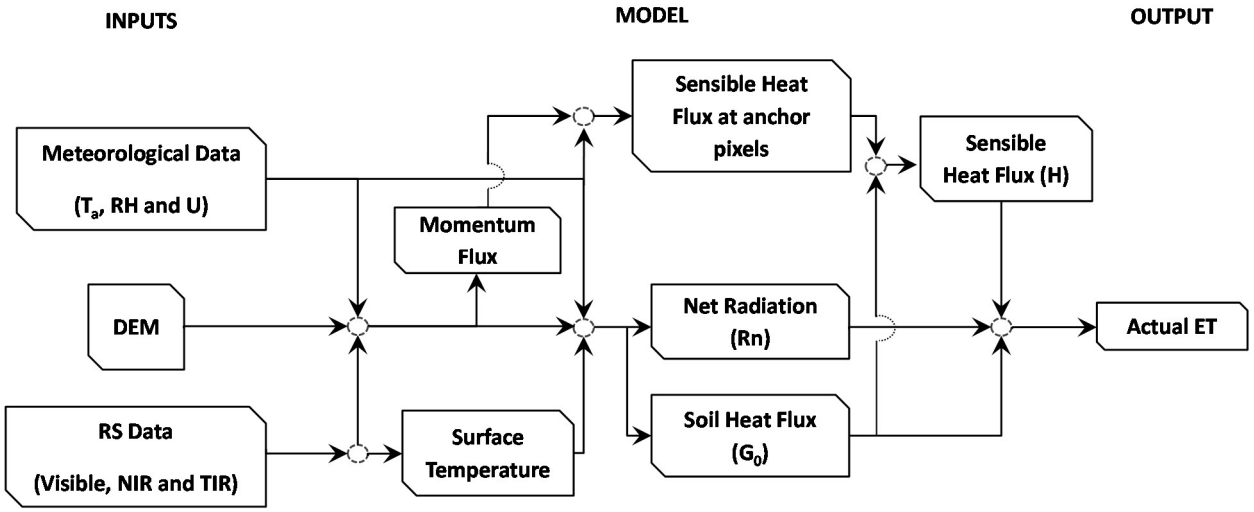

Figure 2. Flowchart of SEBAL model, main inputs, and output. (U is the wind speed, RH is the relative humidity and Ta is air temperature).

The instantaneous net surface radiation flux R_n (W m^{-2}) at the land surface is estimated from Landsat and meteorological data as a balance of incoming and outgoing radiation fluxes [27,61], as follows:

$$R_n = (1 - \alpha)R_{S\downarrow} + R_{L\downarrow} - R_{L\uparrow} - (1 - \varepsilon_o)R_{L\downarrow} \quad (4)$$

where α is surface albedo (-), $R_{S\downarrow}$ is incoming short-wave radiation (W m^{-2}), $R_{L\downarrow}$ is incoming long-wave radiation (W m^{-2}), $R_{L\uparrow}$ is outgoing long-wave radiation (W m^{-2}), and ε_o is the surface emissivity (-). The term $(1-\varepsilon_o)$ $R_{L\downarrow}$ represents the long-wave radiation reflected from the land surface.

The instantaneous value of soil heat flux, G_0 (W m^{-2}), is estimated from the normalized difference vegetation index, NDVI, the surface radiometric temperature, T_{rad} (°K), α and Rn, as proposed by Bastiaanssen [60]:

$$G_0 = \frac{T_{rad}}{\alpha}(0.0038\alpha + 0.007\alpha^2)(1 - 0.98NDVI^4)R_n \quad (5)$$

Usually the difference between the aerodynamic temperature and the air temperature above the canopy is needed for sensible heat flux calculations. In the SEBAL model, a near-surface temperature gradient (ΔT) is used to obtain H [27,61]:

$$H = \frac{(\rho \times C_p \times \Delta T)}{r_{ah}} \quad (6)$$

where ϱ is air density (kg m^{-3}), c_p is the specific heat of air (J kg^{-1}K^{-1}), r_{ah} is the aerodynamic resistance to heat transport (s m^{-1}) and ΔT (°K) is the temperature gradient between two reference heights, near-surface and air, that governs the transfer of heat.

The temperature gradient ΔT is scaled as a function of T_{rad}. The model assumes that an image pixel reproduces a homogenous transfer layer and that ΔT varies linearly with T_{rad} in an image scene [27,61]. This approach captures the relative variability in land surface temperature and reduces the need for absolute accuracy in thermal infrared imagery [80]. Initially, SEBAL solves the surface energy balance equation and obtains the value of ΔT at two hydrological extremes, the anchor pixels, where reliable values of the sensible heat flux can be estimated. The first extreme is referred to as the cold pixel and represents non-stressed full ground cover vegetation, where ET is at the potential level. The second, the hot pixel, is usually a dry bare agricultural soil, where ET is near to zero. The temperature gradient at the cold pixel (ΔT_{cold}, Equation (7)) is determined by solving the energy balance assuming the ET is near potential and G_0 is negligible. The same procedure is done for the temperature gradient at the hot pixel (ΔT_{hot}, Equation (8)) where the evaporative flux λE_{hot} is considered negligible.

$$\Delta T_{cold} = \frac{(R_{ncold} - \lambda ET_{cold}) \times r_{ah}}{\rho \times c_p} \quad (7)$$

$$\Delta T_{hot} = \frac{(R_{nhot} - G_{0hot}) \times r_{ah}}{\rho \times c_p} \quad (8)$$

The obtained ΔT values at the anchor pixels are used to compute the correlation coefficient a and b of Equation (9) and estimate the T values from the radiometric temperature (T_{rad}) across the whole image scene:

$$\Delta T = aT_{rad} + b \quad (9)$$

SEBAL then retrieves the H at each pixel based on ΔT and estimates the instantaneous latent heat flux λE (W m^{-2}) as a residual of the surface energy balance:

$$\lambda ET = Rn - H - G_0 \quad (10)$$

2.5. Upscaling Instantaneous to Daily Evapotranspiration

Three different methods are used to upscale the instantaneous λE at the satellite overpass time to the daily actual evapotranspiration values.

The first method upscales λE based on the self-preservation of the evaporative fraction [41,61,72]. The instantaneous evaporative fraction (Λ_s) is obtained by SEBAL as the ratio of latent heat flux to the available energy at the land surface:

$$\Lambda_s = \frac{\lambda E}{Rn - G_0} \quad (11)$$

The evaporative fraction's self-preservation means that the ratio of the daily energy fluxes is consistent and invariable during daytime. The daily upscaling is a straightforward approach, as the Λ instantaneous value is supposed to be representative of the average daytime value under fair weather conditions (the so-called daytime self-preservation) [28,68,69,81]. The Λ_s is used to upscale instantaneous λE to the actual evapotranspiration on the image acquisition day, as follows:

$$ET_{D,\Lambda} = \Lambda_S \frac{Rn_{24} - G_{24}}{\lambda \rho_W} \quad (12)$$

where $ET_{D,\Lambda}$ (mm d^{-1}) is the actual daily evapotranspiration upscaled by Λs, R_{n24} (MJ m^{-2} d^{-1}) is the net daily radiation estimated by the procedure outlined in the FAO Irrigation and Drainage Paper No. 56 [82], G_{24} is the daily soil heat flux considered to be zero on a daily basis by SEBAL, λ (MJ m^{-3}) is the latent heat of vaporization and ϱ_w (kg m^{-3}) is the water density.

The second method uses the standardized reference evapotranspiration as an upscaling variable [70,71]. Both instantaneous reference evapotranspiration, $ET_{r,i}$ (mm h^{-1}), and

daily reference evapotranspiration, $ET_{r,24}$ (mm d^{-1}), were computed by meteorological data following the FAO-56 Penman–Monteith method [82]. This method uses an approach similar to the crop coefficient (K_c) concept [82] and assumes proportionality between the ratio of daily to instantaneous actual and reference ET. This proportionality yields a relatively invariable reference evaporative fraction (EF_r), defined as the ratio of the hourly instantaneous actual evapotranspiration, $ET_{a,i}$ (mm h^{-1}), to the corresponding $ET_{r,i}$. The upscaling method uses EF_r to obtain the daily actual evapotranspiration, as follows:

$$ET_{D,EFr} = EF_r \cdot ET_{r,24} = \frac{ET_{a,i}}{ET_{r,i}} ET_{r,24} \quad (13)$$

where $ET_{D,EFr}$ (mm d^{-1}) is the actual daily evapotranspiration upscaled by EF_r.

The third upscaling method uses shortwave radiation as the upscaling variable. The incoming shortwave radiation, $Rs_{\downarrow}$, which is the main source of energy for evapotranspiration at the daily scale [72,73], is used as a reference integration variable, and under the hypothesis of proportionality between changes in ET and $Rs_{\downarrow}$ at the daily scale. This approach also assumes the preservation of the ratio of daily to instantaneous actual ET and the Rs_{24}/Rs_i ratio during daytime hours**:**

$$ET_{D,Rs} = \lambda E \frac{Rs_{24}}{\lambda Rs_i} \quad (14)$$

where Rs_i is instantaneous incoming shortwave radiation, and Rs_{24} is the daily incoming shortwave radiation measured by the micrometeorological station.

2.6. SEBAL Data Extraction

The procedure for comparing SEBAL surface fluxes and ground observations considers the scale mismatch between the EC flux footprint and Landsat pixels. The SEBAL values near the acquisition time outputs were extracted for the study area with elliptical polygons (GIS shapefiles) that extend 100 m from the eddy covariance station and fall into line with the measured footprint orientation (upwind direction). The extracted value is the average of a few pixels (from 4 to 10) falling within the polygons. The polygon extension was chosen to partially match the coarser spatial resolution of Landsat TIR and to exclude the interference of the pine forest and the sea near the tower, which exist respectively at 125 and 200 m from the EC tower (Figure 1).

3. Results and Discussions

3.1. Measured Energy Fluxes

The wind direction, measured clockwise from the north, ranged from 17.28° to 355°, with an average of 218.4°, during the Landsat image acquisition days (Table 1), indicating that measured turbulent fluxes mainly originated from the North-East. The footprint length representing 90% of the total fluxes ($FP_{0.90}$) was, on average, 217 m, with a standard deviation of ±58.29 m. The average length of the footprint peak, representing the source area where the majority of turbulent fluxes originates, was approximately 11.43 m with a standard deviation of ±3.07 m. As such, most of the flux contribution originated from an area smaller than a single Landsat image pixel and covered by Mediterranean maquis, which adds confidence to the footprint–pixel data comparison.

The 30 minutes' energy balance components Rn, H, G_0 and λE were analyzed using the flux tower data in all the Landsat image acquisition days (Table 1). Three dates (DOY 67 of 2009, 118 of 2010 and 257 of 2014) were selected to show the results from different seasons and years (Figure 3). These dates were selected based on the absence of significant data gaps. As shown in Figure 3, Rn exhibited a smooth sinusoidal shape, indicating clear sky for the selected days, with the peak between 12:00 and 14:00. The other fluxes relatively followed the variations of Rn. The sensible heat flux H was the dominant energy component after Rn during the daytime, while λE showed relatively lower values, indi-

cating a limited water availability for the ET process. Negative soil heat fluxes in the afternoon were mainly due to vegetation shading on some soil heat plates. The energy balance closure on the three considered days was acceptable on a daily basis, with an average closure error of less than 15% [64]. The energy balance closure at the near-acquisition time (at 10:00 UTC) was also satisfactory, with C_R of 0.835, 1.04 and 1.05 for the DOY 67-2009, 118-2010 and 257-2014, respectively (the red filled squares on Figure 3b,d,f). Table 2 shows the near-acquisition time C_R, the slope of linear regression equation and the coefficient of determination, describing the diurnal variation of turbulent fluxes with respect to available energy on all the selected image acquisition days. The results were similar to those in the three selected days presented in Figure 3. As shown in Figure 3 and Table 2, the 30 min balance closure was sometimes less satisfactory. The partial closure failure in the open field energy balance measurements could be due to different causes. Some terms of the balance, such as the metabolic and the storage terms (i.e., the energy used for biomass production, metabolic activity, and heat storage in vegetation), are usually not accounted for, and therefore contribute to the global error [83]. Another contributing factor is the land heterogeneity [84]. Although the instrumentation functioning and calibration were checked before measurements, errors due to the partial malfunctioning of sensors and/or human causes can contribute to the partial energy balance unclosure. Closure failure also depends on the scale mismatch of the source areas of the energy components and the flux averaging period [85]. Masseroni et al. [86] showed that an averaging period of 30 min may miss the temporal scale variability, particularly in the case of turbulent fluxes.

Table 2. The near-acquisition time C_R, the slope of linear regression equation and the coefficient of determination of diurnal C_R on the selected LS5 and LS8 image acquisition days.

Year	DOY	C_R at Near-Image Acquisition Time (At 10:00)	Slope of Linear Regression Equation of Diurnal C_R (Zero Intercept)	Coefficient of Determination (R^2)
2009	67	0.83	0.92	0.92
2009	131	1.13	1.05	0.73
2009	170	0.83	0.77	0.85
2009	202	1.18	1.1	0.84
2009	211	1.05	0.96	0.86
2009	218	1.01	1.04	0.8
2009	227	0.94	0.91	0.59
2009	234	1.04	0.96	0.81
2009	243	0.84	0.91	0.85
2009	250	0.81	0.84	0.87
2009	275	1.04	0.87	0.95
2010	118	1.04	1.05	0.91
2010	198	1.36	1.06	0.69
2010	310	0.78	0.86	0.92
2013	222	1.07	1.03	0.64
2013	302	1.05	0.99	0.96
2014	161	1.36	1.1	0.56
2014	209	0.87	1.11	0.78
2014	257	1.05	1.12	0.93

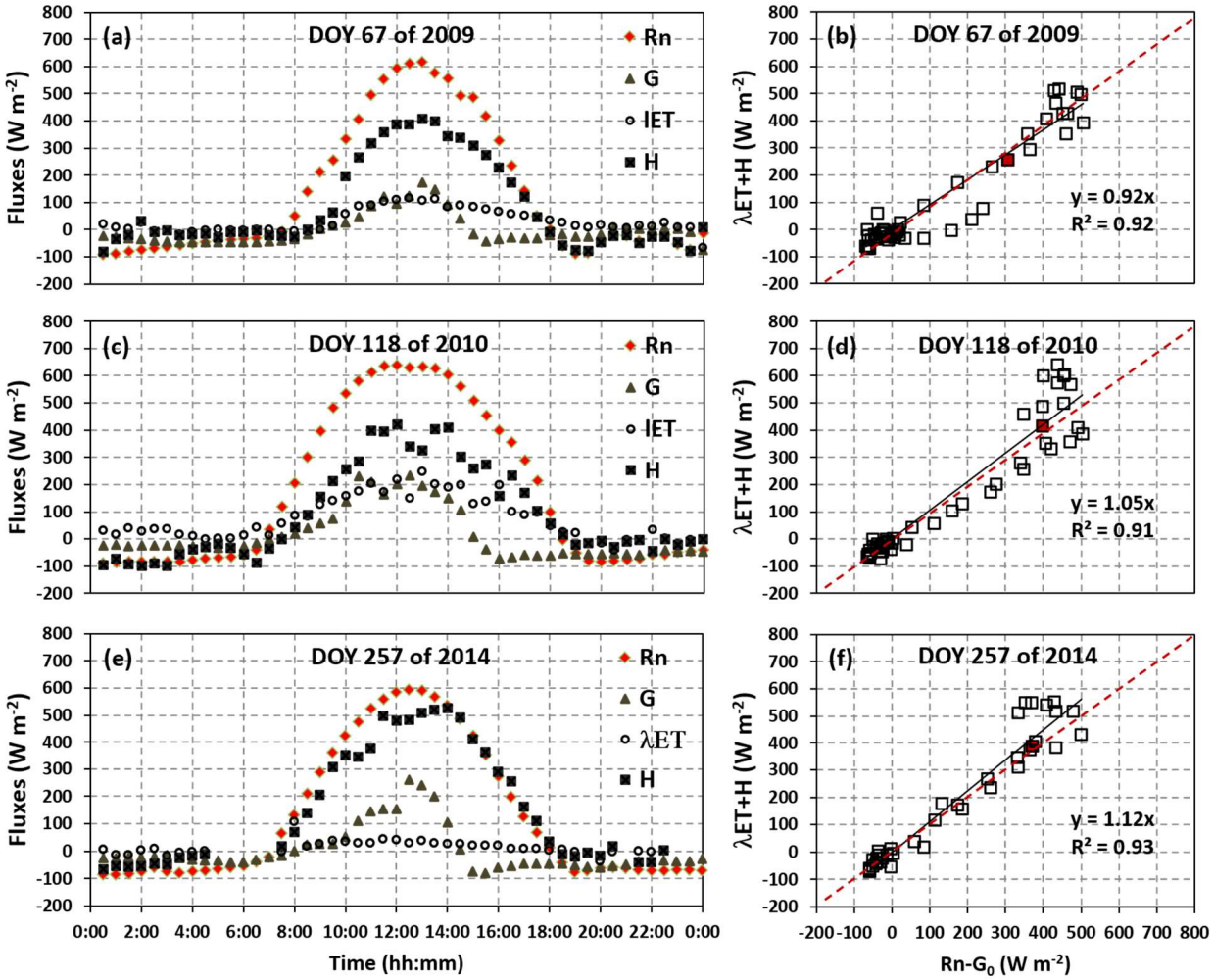

Figure 3. (**a**,**c**,**e**) Daily variation in 30 min surface energy balance components (Rn, G_0, λE and H). (**b**,**d**,**f**) The diurnal energy balance closure on DOY 672009, 1182010 and 2572014, respectively. The red-filled squares represent the energy budget closure near the image acquisition time (at 10:00). The red dashed line is the 1:1 line.

3.2. Diurnal Self-Preservation and Performance of Tower-Derived Upscaling Factors

In this section, we evaluate the validity of the daytime preservation of the upscaling factors, Λ EF_r and Rs_{24}/Rs_i. In-situ flux observations were used to obtain the diurnal variation of the three considered upscaling factors. The 30 min diurnal variation of these factors is shown in Figure 4 for three Landsat acquisition days, DOY 67-2009, 118-2010 and 257-2014, and similar results were found in the rest of the selected image acquisition days. Regarding the tower-derived evaporative fraction (Λ_T), the diurnal variations showed a typical concave-up shape with two peaks, close to sunrise and sunset. Although λET and the available energy, Rn–G_0, varied significantly during the day (Figure 3), Λ_T showed relative conservation during the daytime, which supports the self-preservation hypothesis approximately from 9:00 to 18:00. Here the Λ_T self-preservation can be attributed to several factors, including the relative magnitude of turbulent heat fluxes, and moreover the daytime shape of Λ_T was mainly linked to the amplitude and the phase differences between H and λE (Figure 3). This was confirmed by Gentine et al. [81], who found Λ_T mostly independently of the major forcing factors, namely incoming solar radiation and wind speed. The EF_r upscaling factor trend was generally in line with the Λ_T behavior, as EFr showed relative stability during the daytime, and varied near sunset and sunrise. This is mainly due to the fact that both EF_r and Λ_T take into account the partitioning of latent

energy to the available energy. However, the EF_r factor includes additional instantaneous (half-hourly) meteorological variables that are incorporated in the Penman–Monteith equation. The trend of Rs_{24}/Rs_i also showed low variability and relative consistency during the daytime. Similar to Λ_T, Rs_{24}/Rs_i showed a concave-up shape with peaks near sunrise and sunset. However, compared to Λ_T and EF_r, the Rs_{24}/Rs_i showed more considerable diurnal variability, with higher Rs_{24}/Rs_i values in the early morning (from 7:30 to 8:30 UTC) and late afternoon (from 17:00 to 20:00 UTC) due to relatively low Rs_i values at these time intervals.

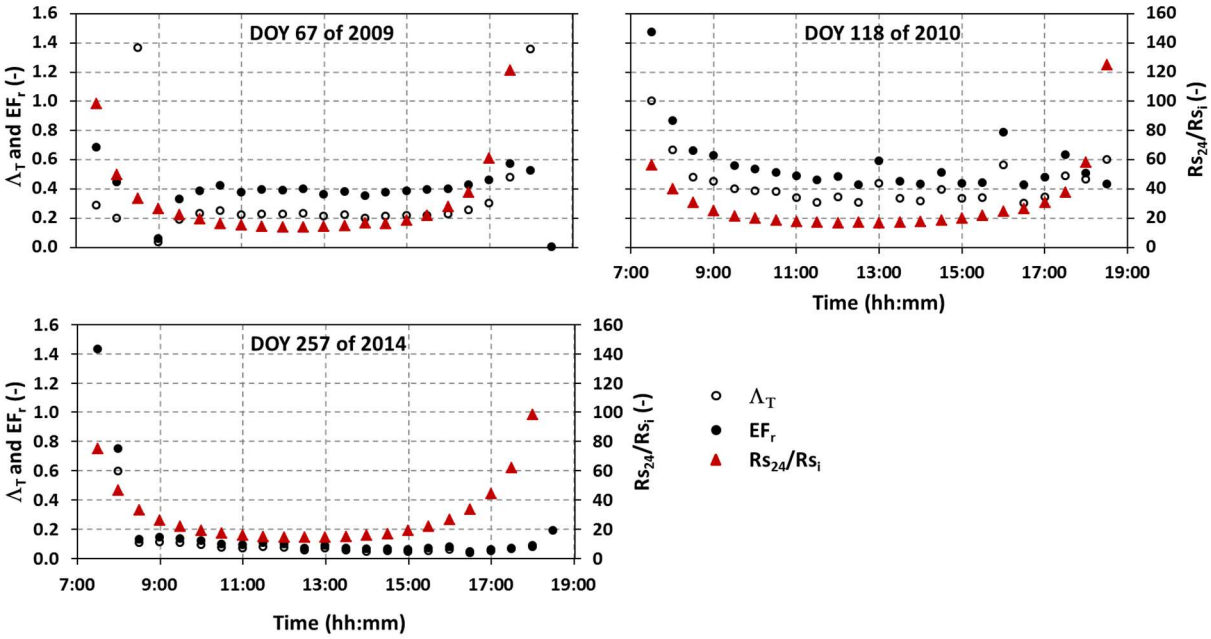

Figure 4. Daytime temporal variability of 30 min scaled evaporative fraction (Λ_T), reference evaporative fraction (EF_r) and incoming shortwave radiation flux ratio (Rs_{24}/Rs_i) during DOY 67-2009, 118-2010 and 257-2014.

With the aim of analyzing the potential of the upscaling factors in retrieving daily ET values, the Λ_T, EF_r and Rs_{24}/Rs_i obtained from the ground-based measurements were used to upscale each of the 30 min measured latent energy values, λE or $ET_{a,i}$, to the daily actual evapotranspiration ($ET_{a,D}$). In this analysis, the use of the measured data aims to isolate the upscaling errors from the SEBAL model-specific instantaneous flux estimation errors. Figure 5 shows the diurnal performance of the upscaling methods on the three considered Landsat acquisition days. Each of the estimated $ET_{a,D}$ values was compared to the corresponding measured daily actual evapotranspiration, $ET_{ID,\ EC}$ (black line in Figure 5). The upscaling methods yielded good $ET_{a,D}$ results near the satellite overpass time (at 10:00 UTC) with errors lower than a threshold of ±15% corresponding to EC closure error tolerability [64] (red dashed lines in Figure 5). For example, the near acquisition time $ET_{a,D}$ estimation errors were 9.6, 5.3 and 3.5% for the Λ_T method, 0.07, 1.2 and 7.9% for the EF_r method and 11.3, 11.3 and 9% for the Rs_{24}/Rs_i method on DOY 67-2009, 257-2014 and 118-2010, respectively (Figure 5). The performance of the three upscaling methods on all the selected image acquisition days (Table 1) was also demonstrated by box and whisker plots (Figure 6). The results show that beyond the satellite overpass time, the upscaled $ET_{a,D}$ values derived by the EF_r and Λ_T methods behave similarly, remaining within or near the tollerance limits for most of the daytime, and significantly falling out of those limits near dawn and sunset. Moreover, some outliers were possible during the daytime. An example can be seen at 8:30 and 9:00 of DOY 67-2009 (Figure 5) due to the significant instantaneous energy closure error and the possible data correction failure where the Bowen ratio could not reproduce the actual energy balance partitioning. Another outlier is shown at 16:00 of

DOY 118-2010, and can be attributed to the unexpected shift of phase differences between H and λE observable at that time (Figure 3). Regarding the Λ_T method, the results showed a wide time window where ET upscaling could be accepted. The applicability is mainly limited to daylight hours (i.e., about between 8:30 and 17:00 for the shown dates), as also indicated by other researchers who showed the method's limitations at dawn or sunset, and at night when the energy fluxes are relatively low, and the advective fluxes are strong [87,88]. The EF_r method performed similarly; however, EF_r showed a wider temporal window of applicability especially in the late afternoon (i.e., between 17:30 and 18:30 DOY 67-209 and 257-2014).This was in line with other studies showing that the EF_r method yields good $ET_{a,D}$ estimations even in the afternoon under advective conditions [26,71]. Using the Rs_{24}/Rs_i values determined during the midday hours slightly underestimated $ET_{a,D}$. This could be due to the more significant increase in Rs_i in this period compared to λE (Equation (14)). On average, the upscaling factors Λ_T, EF_r and to a lower extent Rs_{24}/Rs_i yielded good $ET_{a,D}$ estimations. The upscaling methods based on the preservation hypothesis were valid only during daytime, with some exceptions near dawn and sunrise. However, such a limitation generally does not hinder the applicability because at night, except for rare cases, the latent heat flux is negligible [89,90].

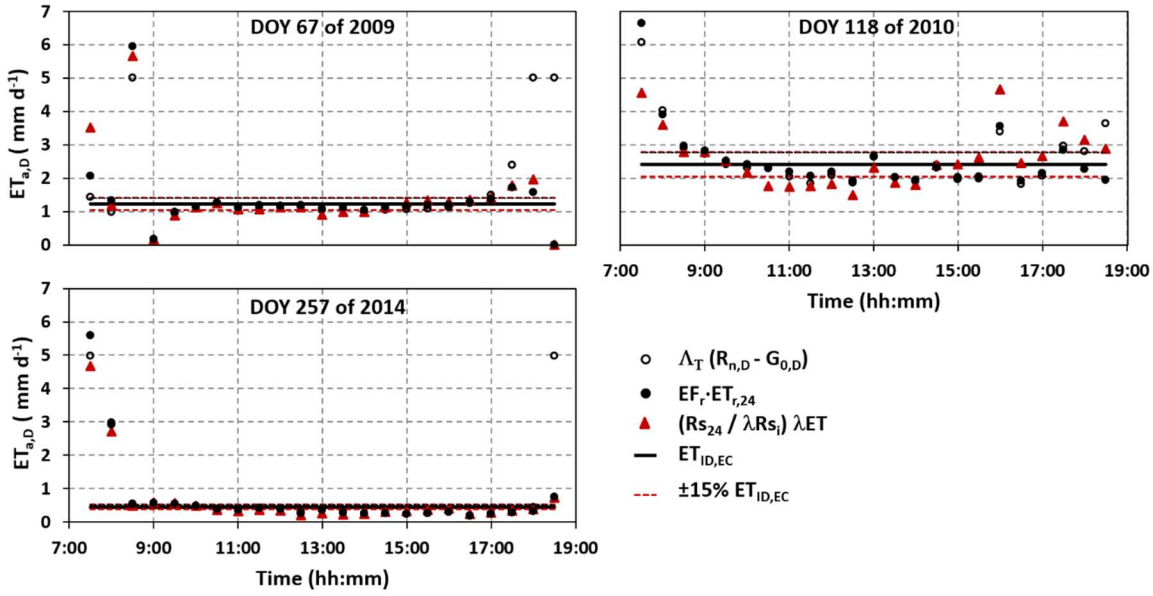

Figure 5. Daytime temporal variability of 30 min tower-derived and upscaled $ET_{a,D}$ based on Λ_T, ET_r and Rs_{24}/Rs_i, and EC measured daily actual ET ($ET_{ID,EC}$) during DOY 67-2009, 118-2010 and 257-2014. The red dashed lines indicate a ±15% $ET_{ID,EC}$ interval.

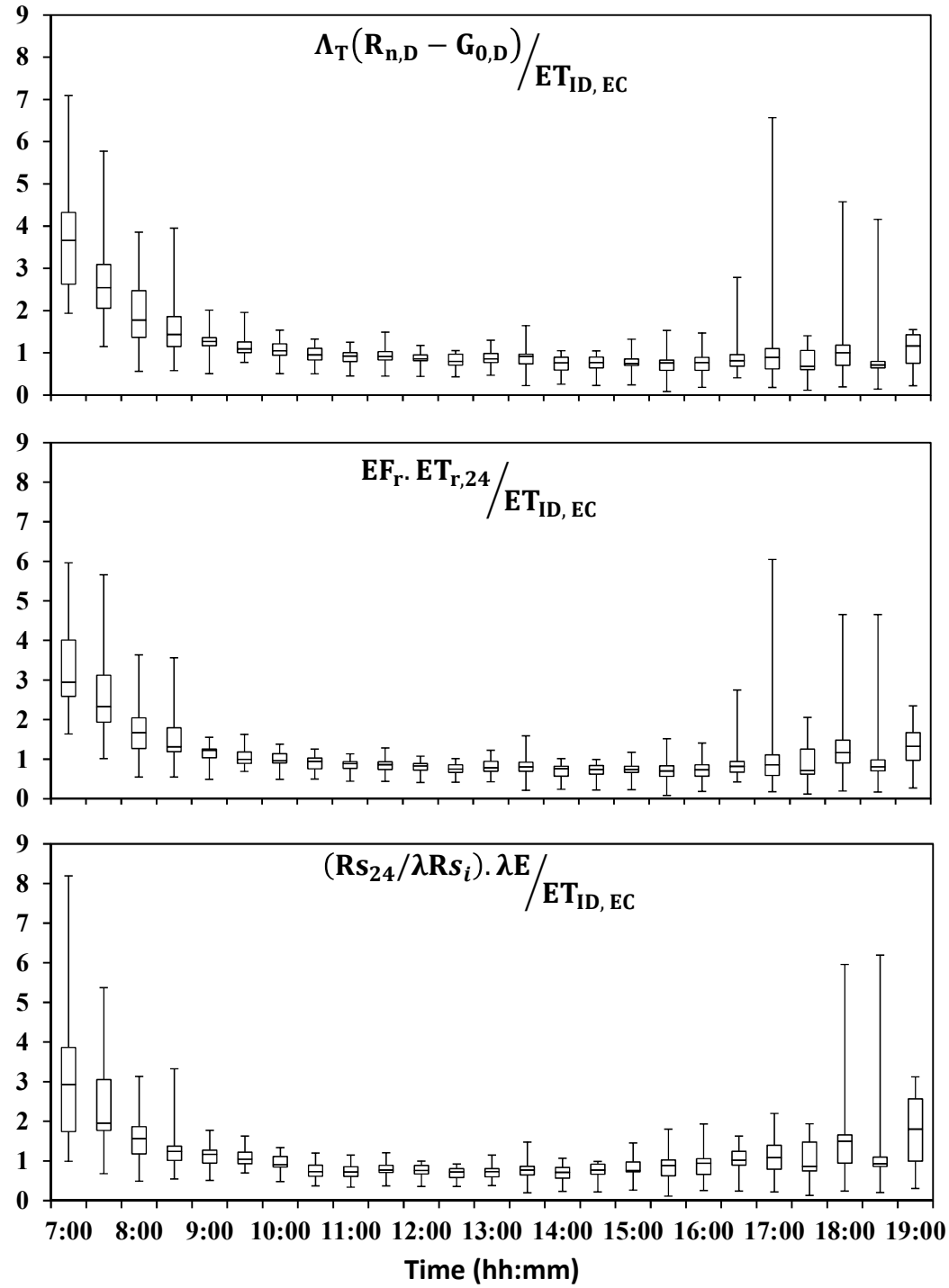

Figure 6. Box and whisker plot for the 30 min temporal variability of the ratio of tower-derived and upscaled $ET_{a,D}$ based on Λ_T, ET_r and Rs_{24}/Rs_i to the EC measured daily actual ET ($ET_{ID, EC}$). The boxes show first (25th percentile), second (median), and third quartiles (75th percentile), and whiskers represent the minimum and maximum values.

Figure 7 compares the daily actual evapotranspiration estimated by upscaling the near overpass time measured latent energy (at 10:00 UTC) to the eddy covariance measured actual daily evapotranspiration ($ET_{ID, EC}$). The results showed that the Λ_T, EF_r and Rs_{24}/Rs_i scaling approaches yielded good $ET_{a,D}$ estimates. The three methods performed

very similarly with coefficients of determination (R^2) greater than 0.75. On average, all the three methods yielded $ET_{a,D}$ estimations that fall within the tolerability range of ±15%. The Λ_T and Rs_{24}/Rs_i methods outperformed the EF_r method, providing results closer to the equity line, while EF_r tends to slightly overestimate $ET_{a,D}$. The results gave more confidence to the applicability of these upscaling methods near the Landsat image acquisition time (between 9:52 and 10:06 UTC). The performed analysis further supported the hypothesis of the upscaling factors' daytime self-preservation. Moreover, the results indicated that the upscaling variables retrieved near the Landsat overpass time could estimate the daily actual evapotranspiration in this natural Mediterranean ecosystem. Our findings agree with other studies that successfully validated the considered upscaling methods in agricultural lands [66,69,70,72,73]. Regarding single acquisition days, some estimation errors can be noticed. In such cases it is difficult to give a definitive explanation for the source of errors because the results are strongly dependent on the instantaneous energy balance closure, the diurnal variability of this imbalance and the performance of the correction technique used. Nevertheless, we think that such uncertainties cannot be avoided, and the effects of SEB closure and the correction process are beyond the scope of the current study.

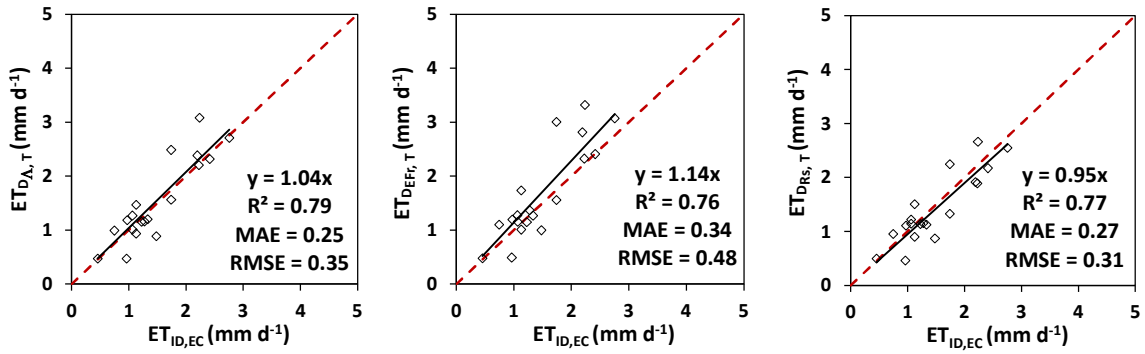

Figure 7. Eddy covariance measured actual daily evapotranspiration ($ET_{ID,\ EC}$) vs. tower-derived upscaled actual daily evapotranspiration based on the Λ scaling factor ($ET_{D\ \ T}$), EF_r scaling factor ($ET_{DEFr,T}$) and Rs_{24}/Rs_i scaling factor ($ET_{DRs,T}$) during the images acquisition days. The red dashed lines represent the 1:1 lines. MAE and RMSE represent the mean absolute error and the root mean square error in mm d^{-1}, respectively.

3.3. Validation of the SEBAL model

The SEBAL model estimates the instantaneous surface energy balance components at the Landsat overpass time. Generally, the measured fluxes and particularly the H and λE are integrated over time. The IT-Noe station-measured fluxes were integrated and provided on a half-hourly basis, which makes the comparison with instantaneous RS-retrieved surface energy fluxes improper. To overcome this inconsistency, similarly to the approach proposed by Bastiaanssen et al. [37], the surface flux ratios that were proven to have diurnal stability were selected as a basis to validate the RS retrieved instantaneous surface energy fluxes. The evaporative fraction estimated by SEBAL (Λ_S) was compared to the EC tower-derived evaporative fractions (Λ_T) for all the selected satellite acquisitions. The results showed that the model estimated Λ with reasonable accuracy, with an R^2 of 0.77, an RMSE of 0.08 and an MAE of 0.05 (Figure 8).

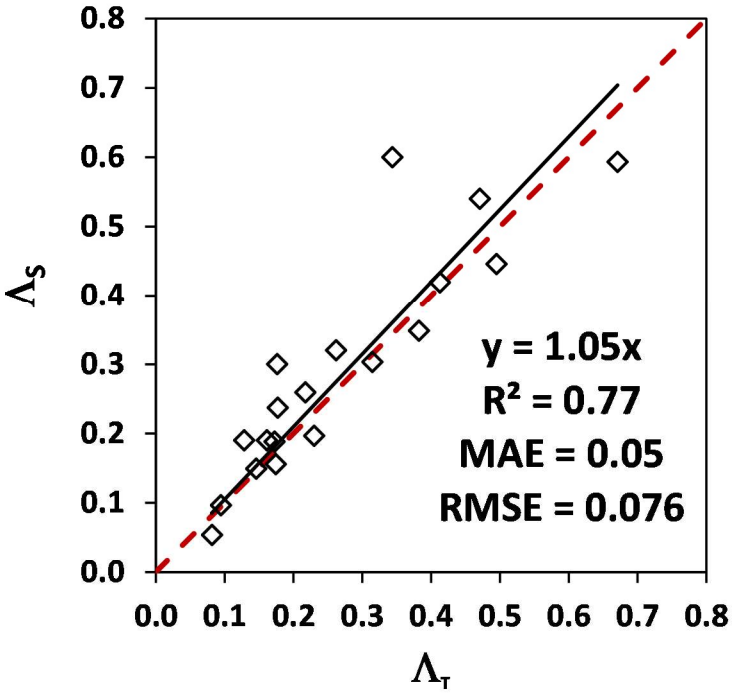

Figure 8. SEBAL-based evaporative fraction (Λ_S) compared to tower-derived evaporative fractions (Λ_T). The red dashed line represents the 1:1 equity line.

Considering single acquisition days, we can observe few cases where the Λ_S is significantly overestimated. An example is the outlier in Figure 8 that refers to DOY 161 of 2014 (Λ_S = 0.6; Λ_T = 0.34). On this particular day, in addition to the SEBAL estimation error, the uncertainties can also be attributed to the energy flux measurements at the near-acquisition time and the energy balance closure errors where the Bowen ratio failed in representing real flux partitioning. In fact, even if the daytime energy balance closure was satisfactory (Cr = 1.1) on DOY 161 of 2014, it was not the case at the near-acquisition time (Cr = 1.36). Excluding this outlier from the data comparison gives R^2, MAE and RMSE values of 0.87, 0.04 and 0.05, respectively.

The Λ_S, EF_r and Rs_{24}/Rs_i factors were used to upscale the SEBAL-estimated instantaneous actual λE to the daily ET. In this case the EF_r fraction was obtained from the SEBAL-retrieved instantaneous available energy, near overpass time and daily ancillary measured meteorological data. The Rs_{24} was measured by the micrometeorological station and Rs_i was estimated from the SEBAL at overpass time. The performance of the upscaling methods is also evaluated here. The upscaled $ET_{a,D}$ was compared to the EC measured daily actual evapotranspiration ($ET_{ID,\ EC}$) (Figure 9). The Λ and Rs_{24}/Rs_i methods showed similar performances, as they slightly overestimated the daily actual evapotranspiration. The EFr scaling factor significantly overestimated the ET data, particularly for values greater than 1.5 mm d^{-1}.

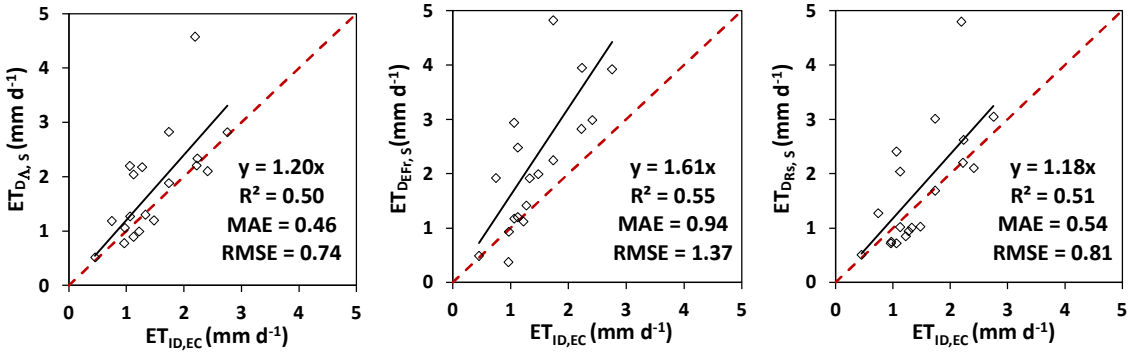

Figure 9. Eddy covariance measured evapotranspiration ($ET_{ID,\ EC}$) and SEBAL estimated evapotranspiration based on Λ scaling factor ($ET_{D\Lambda,\ S}$), EF_r scaling factor ($ET_{DEFr,\ S}$) and Rs_{24}/Rs_i scaling factor ($ET_{DRs,\ S}$) during the images acquisition days. The red dashed line represents the 1:1 line.

Although the SEBAL model showed good instantaneous surface energy flux estimations at the overpass time (as suggested by the Λ comparison done in Figure 8), we observe a decline in performance when comparing the daily upscaled $ET_{a,D}$ to $ET_{ID,\ EC}$. Here, it is important to consider that the $ET_{a,D}$ embeds both instantaneous flux estimations errors and upscaling methods errors. In fact, comparing the performance of upscaling factors obtained from SEBAL (Figure 9) to those obtained from ground-based data (Figure 7) showed that the model-derived factors introduced $ET_{a,D}$ overestimation and increased error indices. Besides the errors arising from the model estimations and the upscaling approaches, uncertainties in the comparison between simulated data and measured data are dependent on the energy closure errors and the failure of the SEB budget correction. This can be manifested in the analysis done by using only in-situ measured data (Figure 7), wherein errors were attributed to the self-preservation of upscaling factors and to both instantaneous and accumulated daily surface energy balance closure errors. In fact, although comparing the overall performance of tower-derived upscaling factors in retrieving actual daily evapotranspiration (Figure 7) showed a satisfactory performance, single-day basis errors cannot be avoided.

We consider positively the results obtained by the Λ and Rs_{24}/Rs_i upscaling factors, taking into consideration the particular complications of applying an SEB model in such a complex natural ecosystem in dry conditions. These include difficulties in simulating the actual ET values of surfaces characterized by high heterogeneity (i.e., high variable ground cover), which is typical to the maquis, particularly the maquis of the studied site that is characterized by variable sized patches of mixed species. This surface heterogeneity adds complexity and can be misrepresented in the Landsat 5 and 8 single pixels, especially in the course TIR spatial resolution (120 and 100 m). Some SEB models were developed to partition the energy fluxes and the surface temperature between canopy and soil; an example is the two-source energy balance model (TSEB) model [30,91–93]. The two-source modeling approach may overcome the single-source SEB model, which deals with a pixel as one transfer layer, especially in areas characterized by non-full vegetation cover. However, we think that the complexity and the heterogeneity of the maquis ecosystem is far beyond the partitioning fluxes between soil and vegetation. In fact, the land surface heterogeneity complication even manifests in ground-based measurements. Stoy et al. [77] analyzed energy balance closure across 173 ecosystems in the FLUXNET database and showed that the worst average energy balance closures (0.70–0.78) were in deciduous broadleaf forests, mixed forests and wetlands, due to landscape heterogeneity.

4. Conclusions

Surface energy balance models combined with free or low-cost remote sensing data were widely used in estimating evapotranspiration in agricultural landscapes. However, an information gap in the application of these models in natural ecosystems still exists. The general objective of this study was to assess the potential of the one-source SEBAL model coupled with Landsat images in simulating the daily actual ET over a coastal Mediterranean maquis.

The SEBAL model firstly estimates the instantaneous latent heat fluxes at the satellite overpass-time, then upscales these instantaneous values to daily values. In this study we used the Λ, ET_r and Rs_{24}/Rs_i upscaling factors under the assumption of diurnal preservation. An analysis performed with in-situ measured data confirmed that the self-preservation of Λ, ET_r and Rs_{24}/Rs_i was assured during daytime. Moreover, the comparison between tower-derived and upscaled daily actual ET with eddy covariance measured daily actual evapotranspiration indicated a significant time window wherein the upscaling approaches were effective, and these were mainly limited to daylight hours. This supported the application of the upscaling approaches in the selected Landsat scene acquisition time (near 10:00 UTC). The comparison of the simulated instantaneous evaporative fractions with the ones obtained from half-hour integrated tower data, provided at the near-overpass time, showed that the SEBAL model could efficiently reproduce the instantaneous energy fluxes. However, when the upscaled daily ET values obtained from the SEBAL instantaneous latent heat fluxes were compared to the measured ET values, the efficiency of the model tended to decrease. This was due to the superimposition of the model instantaneous flux estimation errors with the upscaling methods errors. Moreover, uncertainties in the comparison can be attributed to both instantaneous (at the near overpass time) and daily surface energy balance closure errors. Generally, the Λ and Rs_{24}/Rs_i were more efficient in estimating daily ET compared to the ET_r upscaling approach, which significantly overestimated the daily evapotranspiration. Moreover, compared to the first two methods the EF_r approach requires additional meteorological inputs both at the instantaneous (half-hourly or hourly) and the daily scale. Based on our results, the Λ and Rs_{24}/Rs_i methods are recommended for ET estimation over heterogeneous natural landscapes such as the maquis environment investigated in this study. Furthermore, future applications could also benefit from the remote sensing of incoming shortwave radiation ($Rs_\downarrow$) required in the Λ and Rs_{24}/Rs_i upscaling methods. Currently, $Rs_\downarrow$ data can be obtained with relatively high accuracy by geostationary satellites [94,95]. This reduces the dependence on ground data and provides further opportunities for SEBAL large-scale applications in natural areas characterized by data scarcity.

The study demonstrated that the SEBAL model with the Landsat moderate spatial resolution data can estimate the actual evapotranspiration of maquis in a semiarid natural Mediterranean environment with relatively acceptable reliability, taking into consideration the complexity of the studied ecosystem. Such application represents a valuable tool, which better represents the spatial and temporal variability of ET. This spatialized data by itself, or integrated into hydrological modeling, can be a great resource for environmental studies and water resources management.

Author Contributions: H.A. developed the hydrological analysis. M.P., S.M. and C.S. acquired and provided the field data that were processed by H.A., S.D.P. and F.G.; M.P. and D.S. coordinated the team and supervised the research. All the authors analyzed the results and contributed to write and to revise the manuscript. All authors have read and agreed to the published version of the manuscript.

Funding: This Research was funded by Regione Autonoma Sardegna in the framework of the *HYDROSARD* project and the University of Sassari research fund FAR2020SIRCACB, FAR2019PIRASTRU and FAR2020PIRASTRUMA.

Acknowledgments: This research was developed in the framework of the *HYDROSARD* project and was carried out at the Department of Agriculture of the University of Sassari. The authors

would like to acknowledge the financial support of the Regione Autonoma Sardegna for funding the project. Authors would also like to acknowledge the University of Sassari 2020 research fund FAR2020SIRCACB, FAR2019PIRASTRU and FAR2020PIRASTRUMA.

Conflicts of interest: The authors declare no conflict of personal relationships or competing financial interests that could have influenced the work reported in this paper.

References

1. Wagener, T.; Sivapalan, M.; Troch, P.A.; McGlynn, B.L.; Harman, C.J.; Gupta, H.V.; Kumar, P.; Rao, P.S.C.; Basu, N.B.; Wilson, J.S. The Future of Hydrology: An Evolving Science for a Changing World. *Water Resour. Res.* **2010**, *46*, 46, doi:10.1029/2009WR008906.
2. Chen, L.; Wang, L.; Ma, Y.; Liu, P. Overview of Ecohydrological Models and Systems at the Watershed Scale. *IEEE Syst. J.* **2015**, *9*, 1091–1099, doi:10.1109/JSYST.2013.2296979.
3. Vicente-Serrano, S.M.; Beguería, S.; López-Moreno, J.I. A Multiscalar Drought Index Sensitive to Global Warming: The Standardized Precipitation Evapotranspiration Index. *J. Clim.* **2010**, *23*, 1696–1718, doi:10.1175/2009JCLI2909.1.
4. Spano, D.; Snyder, R.L.; Sirca, C.; Duce, P. ECOWAT—A Model for Ecosystem Evapotranspiration Estimation. *Agric. For. Meteorol.* **2009**, *149*, 1584–1596, doi:10.1016/j.agrformet.2009.04.011.
5. Baldocchi, D.; Falge, E.; Gu, L.; Olson, R.; Hollinger, D.; Running, S.; Anthoni, P.; Bernhofer, C.; Davis, K.; Evans, R.; et al. FLUXNET: A New Tool to Study the Temporal and Spatial Variability of Ecosystem-Scale Carbon Dioxide, Water Vapor, and Energy Flux Densities. *Bull. Am. Meteorol. Soc.* **2001**, *82*, 2415–2434, doi:10.1175/1520-0477(2001)082<2415:FANTTS>2.3.CO;2.
6. Aubinet, M.; Vesala, T.; Papale, D. (Eds.) *Eddy Covariance: A Practical Guide to Measurement and Data Analysis*; Springer: Dordrecht, The Netherlands, 2012.
7. Aguilos, M.; Stahl, C.; Burban, B.; Hérault, B.; Courtois, E.; Coste, S.; Wagner, F.; Ziegler, C.; Takagi, K.; Bonal, D. Interannual and Seasonal Variations in Ecosystem Transpiration and Water Use Efficiency in a Tropical Rainforest. *Forests* **2019**, *10*, 14, doi:10.3390/f10010014.
8. Hemakumara, H.M.; Chandrapala, L.; Moene, A.F. Evapotranspiration Fluxes over Mixed Vegetation Areas Measured from Large Aperture Scintillometer. *Agric. Water Manag.* **2003**, *58*, 109–122, doi:10.1016/S0378-3774(02)00131-2.
9. Wesely, M.L. A Comparison of Two Optical Methods for Measuring Line Averages of Thermal Exchanges above Warm Water Surfaces. *J. Appl. Meteorol.* **1976**, *15*, 1177–1188.
10. Angus, D.E.; Watts, P.J. Evapotranspiration—How Good Is the Bowen Ratio Method? *Agric. Water Manag.* **1984**, *8*, 133–150, doi:10.1016/0378-3774(84)90050-7.
11. Bowen, I.S. The Ratio of Heat Losses by Conduction and by Evaporation from Any Water Surface. *Phys. Rev.* **1926**, *27*, 779–787, doi:10.1103/PhysRev.27.779.
12. Paw, U.K.; Qiu, J.; Su, H.-B.; Watanabe, T.; Brunet, Y. Surface Renewal Analysis: A New Method to Obtain Scalar Fluxes. *Agric. For. Meteorol.* **1995**, *74*, 119–137, doi:10.1016/0168-1923(94)02182-J.
13. Spano, D.; Snyder, R.L.; Duce, P.; Paw, U.K.T. Surface Renewal Analysis for Sensible Heat Flux Density Using Structure Functions. *Agric. For. Meteorol.* **1997**, *86*, 259–271, doi:10.1016/S0168-1923(96)02420-3.
14. Edwards, W.R.N. Precision Weighing Lysimetry for Trees, Using a Simplified Tared-Balance Design. *Tree Physiol.* **1986**, *1*, 127–144, doi:10.1093/treephys/1.2.127.
15. Jensen, M.E.; Burman, R.D.; Allen, R.G. *Evapotranspiration and Irrigation Water Requirements*; ASCE Manuals and Reports on Engineering Practice No. 70: Reston, VA, USA, 1990.
16. Marek, T.H.; Schneider, A.D.; Howell, T.A.; Ebeling, L.L. Design and Construction of Large Weighing Monolithic Lysimeters. *Trans. ASAE* **1988**, *31*, 477–0484.
17. Cuenca, R.H.; Stangel, D.E.; Kelly, S.F. Soil Water Balance in a Boreal Forest. *J. Geophys. Res. Atmos.* **1997**, *102*, 29355–29365, doi:10.1029/97JD02312.
18. Eastham, J.; Rose, C.W.; Cameron, D.M.; Rance, S.J.; Talsma, T. The Effect of Tree Spacing on Evaporation from an Agroforestry Experiment. *Agric. For. Meteorol.* **1988**, *42*, 355–368, doi:10.1016/0168-1923(88)90043-3.
19. Granier, A. Une nouvelle méthode pour la mesure du flux de sève brute dans le tronc des arbres. *Ann. For. Sci.* **1985**, *42*, 193–200, doi:10.1051/forest:19850204.
20. Smith, D.M.; Allen, S.J. Measurement of Sap Flow in Plant Stems. *J. Exp. Bot.* **1996**, *47*, 1833–1844, doi:10.1093/jxb/47.12.1833.
21. Droogers, P.; Bastiaanssen, W.G.M.; Beyazgül, M.; Kayam, Y.; Kite, G.W.; Murray-Rust, H. Distributed Agro-Hydrological Modeling of an Irrigation System in Western Turkey. *Agric. Water Manag.* **2000**, *43*, 183–202, doi:10.1016/S0378-3774(99)00055-4.
22. Elhaddad, A.; Garcia, L.A. Surface Energy Balance-Based Model for Estimating Evapotranspiration Taking into Account Spatial Variability in Weather. *J. Irrig. Drain. Eng.* **2008**, *134*, 681–689, doi:10.1061/(ASCE)0733-9437(2008)134:6(681).
23. Mohanty, B.P.; Skaggs, T.H. Spatio-Temporal Evolution and Time-Stable Characteristics of Soil Moisture within Remote Sensing Footprints with Varying Soil, Slope, and Vegetation. *Adv. Water Resour.* **2001**, *24*, 1051–1067, doi:10.1016/S0309-1708(01)00034-3.
24. Waring, R.H.; Running, S.W. *Forest Ecosystems: Analysis at Multiple Scales*, 3rd ed.; Elsevier/Academic Press: Amsterdam, The Netherlands; Boston, MA, USA, 2007; ISBN 978-0-12-370605-8.
25. Jarvis, P.G. Scaling Processes and Problems. *Plant Cell Environ.* **1995**, *18*, 1079–1089, doi:10.1111/j.1365-3040.1995.tb00620.x.

26. Allen, R.G.; Tasumi, M.; Trezza, R. Satellite-Based Energy Balance for Mapping Evapotranspiration with Internalized Calibration (METRIC)—Model. *J. Irrig. Drain. Eng.* **2007**, *133*, 380–394, doi:10.1061/(ASCE)0733-9437(2007)133:4(380).
27. Bastiaanssen, W.G.M.; Menenti, M.; Feddes, R.A.; Holtslag, A.A.M. A Remote Sensing Surface Energy Balance Algorithm for Land (SEBAL). 1. Formulation. *J. Hydrol.* **1998**, *212–213*, 198–212, doi:10.1016/S0022-1694(98)00253-4.
28. Maltese, A.; Awada, H.; Capodici, F.; Ciraolo, G.; La Loggia, G.; Rallo, G. On the Use of the Eddy Covariance Latent Heat Flux and Sap Flow Transpiration for the Validation of a Surface Energy Balance Model. *Remote Sens.* **2018**, *10*, 195, doi:10.3390/rs10020195.
29. Minacapilli, M.; Cammalleri, C.; Ciraolo, G.; Rallo, G.; Provenzano, G. Using Scintillometry to Assess Reference Evapotranspiration Methods and Their Impact on the Water Balance of Olive Groves. *Agric. Water Manag.* **2016**, *170*, 49–60, doi:10.1016/j.agwat.2015.12.004.
30. Norman, J.M.; Kustas, W.P.; Humes, K.S. Source Approach for Estimating Soil and Vegetation Energy Fluxes in Observations of Directional Radiometric Surface Temperature. *Agric. For. Meteorol.* **1995**, *77*, 263–293, doi:10.1016/0168-1923(95)02265-Y.
31. Roerink, G.J.; Su, Z.; Menenti, M. S-SEBI: A Simple Remote Sensing Algorithm to Estimate the Surface Energy Balance. *Phys. Chem. Earth Part B Hydrol. Ocean. Atmos.* **2000**, *25*, 147–157, doi:10.1016/S1464-1909(99)00128-8.
32. Senay, G.B.; Bohms, S.; Singh, R.K.; Gowda, P.H.; Velpuri, N.M.; Alemu, H.; Verdin, J.P. Operational Evapotranspiration Mapping Using Remote Sensing and Weather Datasets: A New Parameterization for the SSEB Approach. *JAWRA J. Am. Water Resour. Assoc.* **2013**, *49*, 577–591, doi:10.1111/jawr.12057.
33. Su, Z. The Surface Energy Balance System (SEBS) for Estimation of Turbulent Heat Fluxes. *Hydrol. Earth Syst. Sci.* **2002**, *6*, 85–100, doi:10.5194/hess-6-85-2002.
34. Wagle, P.; Bhattarai, N.; Gowda, P.H.; Kakani, V.G. Performance of Five Surface Energy Balance Models for Estimating Daily Evapotranspiration in High Biomass Sorghum. *ISPRS J. Photogramm. Remote Sens.* **2017**, *128*, 192–203, doi:10.1016/j.isprsjprs.2017.03.022.
35. Yang, Y.; Scott, R.L.; Shang, S. Modeling Evapotranspiration and Its Partitioning over a Semiarid Shrub Ecosystem from Satellite Imagery: A Multiple Validation. *JARS* **2013**, *7*, 073495, doi:10.1117/1.JRS.7.073495.
36. Awada, H.; Ciraolo, G.; Maltese, A.; Provenzano, G.; Moreno Hidalgo, M.A.; Còrcoles, J.I. Assessing the Performance of a Large-Scale Irrigation System by Estimations of Actual Evapotranspiration Obtained by Landsat Satellite Images Resampled with Cubic Convolution. *Int. J. Appl. Earth Obs. Geoinf.* **2019**, *75*, 96–105, doi:10.1016/j.jag.2018.10.016.
37. Bastiaanssen, W.G.M.; Pelgrum, H.; Wang, J.; Ma, Y.; Moreno, J.F.; Roerink, G.J.; van der Wal, T. A Remote Sensing Surface Energy Balance Algorithm for Land (SEBAL).: Part 2: Validation. *J. Hydrol.* **1998**, *212–213*, 213–229, doi:10.1016/S0022-1694(98)00254-6.
38. Bhattarai, N.; Shaw, S.B.; Quackenbush, L.J.; Im, J.; Niraula, R. Evaluating Five Remote Sensing Based Single-Source Surface Energy Balance Models for Estimating Daily Evapotranspiration in a Humid Subtropical Climate. *Int. J. Appl. Earth Obs. Geoinf.* **2016**, *49*, 75–86, doi:10.1016/j.jag.2016.01.010.
39. Timmermans, W.J.; Kustas, W.P.; Anderson, M.C.; French, A.N. An Intercomparison of the Surface Energy Balance Algorithm for Land (SEBAL) and the Two-Source Energy Balance (TSEB) Modeling Schemes. *Remote Sens. Environ.* **2007**, *108*, 369–384, doi:10.1016/j.rse.2006.11.028.
40. Bastiaanssen, W.G.M.; Brito, R.A.L.; Bos, M.G.; Souza, R.A.; Cavalcanti, E.B.; Bakker, M.M. Low Cost Satellite Data for Monthly Irrigation Performance Monitoring: Benchmarks from Nilo Coelho, Brazil. *Irrig. Drain. Syst.* **2001**, *15*, 53–79, doi:10.1023/A:1017967021198.
41. Bastiaanssen, W.G.M.; Van der Wal, T.; Visser, T.N.M. Diagnosis of Regional Evaporation by Remote Sensing to Support Irrigation Performance Assessment. *Irrig. Drain. Syst* **1996**, *10*, 1–23, doi:10.1007/BF01102762.
42. Senay, G.B.; Schauer, M.; Friedrichs, M.; Velpuri, N.M.; Singh, R.K. Satellite-Based Water Use Dynamics Using Historical Landsat Data (1984–2014) in the Southwestern United States. *Remote Sens. Environ.* **2017**, *202*, 98–112, doi:10.1016/j.rse.2017.05.005.
43. Molden, D.; Sakthivadivel, R. Water Accounting to Assess Use and Productivity of Water. *Int. J. Water Resour. Dev.* **1999**, *15*, 55–71, doi:10.1080/07900629948934.
44. Akbari, M.; Toomanian, N.; Droogers, P.; Bastiaanssen, W.; Gieske, A. Monitoring Irrigation Performance in Esfahan, Iran, Using NOAA Satellite Imagery. *Agric. Water Manag.* **2007**, *88*, 99–109, doi:10.1016/j.agwat.2006.10.019.
45. Al Zayed, I.S.; Elagib, N.A.; Ribbe, L.; Heinrich, J. Spatio-Temporal Performance of Large-Scale Gezira Irrigation Scheme, Sudan. *Agric. Syst.* **2015**, *133*, 131–142, doi:10.1016/j.agsy.2014.10.009.
46. Blatchford, M.L.; Karimi, P.; Bastiaanssen, W.G.M.; Nouri, H. From Global Goals to Local Gains—A Framework for Crop Water Productivity. *ISPRS Int. J. Geo-Inf.* **2018**, *7*, 414, doi:10.3390/ijgi7110414.
47. Zwart, S.J.; Bastiaanssen, W.G.M.; de Fraiture, C.; Molden, D.J. A Global Benchmark Map of Water Productivity for Rainfed and Irrigated Wheat. *Agric. Water Manag.* **2010**, *97*, 1617–1627, doi:10.1016/j.agwat.2010.05.018.
48. Ahmad, M.D.; Kirby, M.; Islam, M.S.; Hossain, M.J.; Islam, M.M. Groundwater Use for Irrigation and Its Productivity: Status and Opportunities for Crop Intensification for Food Security in Bangladesh. *Water Resour. Manag.* **2014**, *28*, 1415–1429, doi:10.1007/s11269-014-0560-z.
49. Ahmad, M.-D.; Bastiaanssen, W.G.M.; Feddes, R.A. A New Technique to Estimate Net Groundwater Use across Large Irrigated Areas by Combining Remote Sensing and Water Balance Approaches, Rechna Doab, Pakistan. *Hydrogeol. J.* **2005**, *13*, 653–664, doi:10.1007/s10040-004-0394-5.

50. Rodell, M.; Velicogna, I.; Famiglietti, J.S. Satellite-Based Estimates of Groundwater Depletion in India. *Nature* **2009**, *460*, 999–1002, doi:10.1038/nature08238.
51. Cammalleri, C.; Agnese, C.; Ciraolo, G.; Minacapilli, M.; Provenzano, G.; Rallo, G. Actual Evapotranspiration Assessment by Means of a Coupled Energy/Hydrologic Balance Model: Validation over an Olive Grove by Means of Scintillometry and Measurements of Soil Water Contents. *J. Hydrol.* **2010**, *392*, 70–82, doi:10.1016/j.jhydrol.2010.07.046.
52. Droogers, P.; Bastiaanssen, W. Irrigation Performance Using Hydrological and Remote Sensing Modeling. *J. Irrig. Drain. Eng.* **2002**, *128*, 11–18, doi:10.1061/(ASCE)0733-9437(2002)128:1(11).
53. Immerzeel, W.W.; Droogers, P. Calibration of a Distributed Hydrological Model Based on Satellite Evapotranspiration. *J. Hydrol.* **2008**, *349*, 411–424, doi:10.1016/j.jhydrol.2007.11.017.
54. Muthuwatta, L.P.; Ahmad, M.-D.; Bos, M.G.; Rientjes, T.H.M. Assessment of Water Availability and Consumption in the Karkheh River Basin, Iran—Using Remote Sensing and Geo-Statistics. *Water Resour. Manag.* **2010**, *24*, 459–484, doi:10.1007/s11269-009-9455-9.
55. Tomaselli, R. The Degradation of the Mediterranean Maquis. *Ambio* **1977**, *6*, 356–362.
56. Palahi, M.; Mavsar, R.; Gracia, C.; Birot, Y. Mediterranean Forests under Focus. *Int. For. Rev.* **2008**, *10*, 676–688, doi:10.1505/ifor.10.4.676.
57. Pirastru, M.; Niedda, M.; Castellini, M. Effects of Maquis Clearing on the Properties of the Soil and on the Near-Surface Hydrological Processes in a Semi-Arid Mediterranean Environment. *J. Agric. Eng.* **2014**, *45*, 176–187, doi:10.4081/jae.2014.428.
58. Folton, N.; Martin, E.; Arnaud, P.; L'Hermite, P.; Tolsa, M. A 50-Year Analysis of Hydrological Trends and Processes in a Mediterranean Catchment. *Hydrol. Earth Syst. Sci.* **2019**, *23*, 2699–2714, doi:10.5194/hess-23-2699-2019.
59. Niedda, M.; Pirastru, M. Field Investigation and Modelling of Coupled Stream Discharge and Shallow Water-Table Dynamics in a Small Mediterranean Catchment (Sardinia). *Hydrol. Process.* **2014**, *28*, 5423–5435, doi:10.1002/hyp.10016.
60. Bastiaanssen, W.G.M. SEBAL-Based Sensible and Latent Heat Fluxes in the Irrigated Gediz Basin, Turkey. *J. Hydrol.* **2000**, *229*, 87–100, doi:10.1016/S0022-1694(99)00202-4.
61. Bastiaanssen, W.G.M.; Noordman, E.J.M.; Pelgrum, H.; Davids, G.; Thoreson, B.P.; Allen, R.G. SEBAL Model with Remotely Sensed Data to Improve Water-Resources Management under Actual Field Conditions. *J. Irrig. Drain. Eng.* **2005**, *131*, 85–93, doi:10.1061/(ASCE)0733-9437(2005)131:1(85).
62. Huntingford, C.; Cox, P.M.; Lenton, T.M. Contrasting Responses of a Simple Terrestrial Ecosystem Model to Global Change. *Ecol. Model.* **2000**, *134*, 41–58, doi:10.1016/S0304-3800(00)00330-6.
63. Minacapilli, M.; Agnese, C.; Blanda, F.; Cammalleri, C.; Ciraolo, G.; D'Urso, G.; Iovino, M.; Pumo, D.; Provenzano, G.; Rallo, G. Estimation of Actual Evapotranspiration of Mediterranean Perennial Crops by Means of Remote-Sensing Based Surface Energy Balance Models. *Hydrol. Earth Syst. Sci.* **2009**, *13*, 1061–1074, doi:10.5194/hess-13-1061-2009.
64. Allen, R.; Irmak, A.; Trezza, R.; Hendrickx, J.M.H.; Bastiaanssen, W.; Kjaersgaard, J. Satellite-Based ET Estimation in Agriculture Using SEBAL and METRIC. *Hydrol. Process.* **2011**, *25*, 4011–4027, doi:10.1002/hyp.8408.
65. Bastiaanssen, W.G.M.; Pelgrum, H.; Soppe, R.W.O.; Allen, R.G.; Thoreson, B.P.; de C. Teixeira, A.H. Thermal-Infrared Technology for Local and Regional Scale Irrigation Analyses in Horticultural Systems. In *Proceedings of the Acta Horticulturae, Leuven, Belgium, 30 June 2008*; International Society for Horticultural Science (ISHS): Mildura, VIC, Australia, 2008; pp. 33–46
66. Cammalleri, C.; Anderson, M.C.; Ciraolo, G.; D'Urso, G.; Kustas, W.P.; La Loggia, G.; Minacapilli, M. Applications of a Remote Sensing-Based Two-Source Energy Balance Algorithm for Mapping Surface Fluxes without in Situ Air Temperature Observations. *Remote Sens. Environ.* **2012**, *124*, 502–515, doi:10.1016/j.rse.2012.06.009.
67. Chávez, J.L.; Neale, C.M.U.; Prueger, J.H.; Kustas, W.P. Daily Evapotranspiration Estimates from Extrapolating Instantaneous Airborne Remote Sensing ET Values. *Irrig. Sci.* **2008**, *27*, 67–81, doi:10.1007/s00271-008-0122-3.
68. Crago, R.D. Conservation and Variability of the Evaporative Fraction during the Daytime. *J. Hydrol.* **1996**, *180*, 173–194, doi:10.1016/0022-1694(95)02903-6.
69. Maltese, A.; Capodici, F.; Ciraolo, G.; Loggia, G.L.; Rallo, G. Assessing Daily Actual Evapotranspiration through Energy Balance: An Experiment to Evaluate the Selfpreservation Hypothesis with Acquisition Time. In Proceedings of the Remote Sensing for Agriculture, Ecosystems, and Hydrology XV, Dresden, Germany, 16 October 2013; International Society for Optics and Photonics: Bellingham, Washington DC, USA, 2013; Volume 8887, p. 888718.
70. Cammalleri, C.; Anderson, M.C.; Kustas, W.P. Upscaling of Evapotranspiration Fluxes from Instantaneous to Daytime Scales for Thermal Remote Sensing Applications. *Hydrol. Earth Syst. Sci.* **2014**, *18*, 1885–1894, doi:10.5194/hess-18-1885-2014.
71. Trezza, R. Evapotranspiration Using a Satellite-Based Surface Energy Balance with Standardized Ground Control. Ph.D. Thesis, Utah State University, Logan, UT, USA, 2002.
72. Jackson, R.D.; Hatfield, J.L.; Reginato, R.J.; Idso, S.B.; Pinter, P.J. Estimation of Daily Evapotranspiration from One Time-of-Day Measurements. *Agric. Water Manag.* **1983**, *7*, 351–362, doi:10.1016/0378-3774(83)90095-1.
73. Zhang, L.; Lemeur, R. Evaluation of Daily Evapotranspiration Estimates from Instantaneous Measurements. *Agric. For. Meteorol.* **1995**, *74*, 139–154, doi:10.1016/0168-1923(94)02181-I.
74. Pastorello, G.; Trotta, C.; Canfora, E.; Chu, H.; Christianson, D.; Cheah, Y.-W.; Poindexter, C.; Chen, J.; Elbashandy, A.; Humphrey, M.; et al. The FLUXNET2015 Dataset and the ONEFlux Processing Pipeline for Eddy Covariance Data. *Sci. Data* **2020**, *7*, 225, doi:10.1038/s41597-020-0534-3.
75. Wilson, K.; Goldstein, A.; Falge, E.; Aubinet, M.; Baldocchi, D.; Berbigier, P.; Bernhofer, C.; Ceulemans, R.; Dolman, H.; Field, C.; et al. Energy Balance Closure at FLUXNET Sites. *Agric. For. Meteorol.* **2002**, *113*, 223–243, doi:10.1016/S0168-1923(02)00109-0.

76. Foken, T. The Energy Balance Closure Problem: An Overview. *Ecol. Appl.* **2008**, *18*, 1351–1367, doi:10.1890/06-0922.1.
77. Stoy, P.C.; Mauder, M.; Foken, T.; Marcolla, B.; Boegh, E.; Ibrom, A.; Arain, M.A.; Arneth, A.; Aurela, M.; Bernhofer, C.; et al. A Data-Driven Analysis of Energy Balance Closure across FLUXNET Research Sites: The Role of Landscape Scale Heterogeneity. *Agric. For. Meteorol.* **2013**, *171–172*, 137–152, doi:10.1016/j.agrformet.2012.11.004.
78. Prueger, J.H.; Hatfield, J.L.; Parkin, T.B.; Kustas, W.P.; Hipps, L.E.; Neale, C.M.U.; MacPherson, J.I.; Eichinger, W.E.; Cooper, D.I. Tower and Aircraft Eddy Covariance Measurements of Water Vapor, Energy, and Carbon Dioxide Fluxes during SMACEX. *J. Hydrometeors* **2005**, *6*, 954–960, doi:10.1175/JHM457.1.
79. Vermote, E.F.; Saleous, N.E.; Justice, C.O.; Kaufman, Y.J.; Privette, J.L.; Remer, L.; Roger, J.C.; Tanré, D. Atmospheric Correction of Visible to Middle-Infrared EOS-MODIS Data over Land Surfaces: Background, Operational Algorithm and Validation. *J. Geophys. Res. Atmos.* **1997**, *102*, 17131–17141, doi:10.1029/97JD00201.
80. Anderson, M.C.; Allen, R.G.; Morse, A.; Kustas, W.P. Use of Landsat Thermal Imagery in Monitoring Evapotranspiration and Managing Water Resources. *Remote Sens. Environ.* **2012**, *122*, 50–65, doi:10.1016/j.rse.2011.08.025.
81. Gentine, P.; Entekhabi, D.; Polcher, J. The Diurnal Behavior of Evaporative Fraction in the Soil–Vegetation–Atmospheric Boundary Layer Continuum. *J. Hydrometeors* **2011**, *12*, 1530–1546, doi:10.1175/2011JHM1261.1.
82. Allen, R.G.; Pereira, L.S.; Raes, D.; Smith, M. *Crop Evapotranspiration—Guidelines for Computing Crop Water Requirements*; Crop Evapotranspiration: Guidelines for Computing Crop Water Requirements; FAO Irrigation and Drainage Paper 56; FAO: Rome, Italy, 1998; p. 15.
83. Foken, T.; Wichura, B. Tools for Quality Assessment of Surface-Based Flux Measurements. *Agric. For. Meteorol.* **1996**, *78*, 83–105, doi:10.1016/0168-1923(95)02248-1.
84. Panin, G.N.; Tetzlaff, G.; Raabe, A. Inhomogeneity of the Land Surface and Problems in TheParameterization of Surface Fluxes in Natural Conditions. *Theor. Appl. Climatol.* **1998**, *60*, 163–178, doi:10.1007/s007040050041.
85. Foken, T.; Wimmer, F.; Mauder, M.; Thomas, C.; Liebethal, C. Some Aspects of the Energy Balance Closure Problem. *Atmos. Chem. Phys.* **2006**, *6*, 4395–4402, doi:10.5194/acp-6-4395-2006.
86. Masseroni, D.; Corbari, C.; Mancini, M. Limitations and Improvements of the Energy Balance Closure with Reference to Experimental Data Measured over a Maize Field. *Atmósfera* **2014**, *27*, 335–352.
87. Brutsaert, W.; Sugita, M. Application of Self-Preservation in the Diurnal Evolution of the Surface Energy Budget to Determine Daily Evaporation. *J. Geophys. Res. Atmos.* **1992**, *97*, 18377–18382, doi:10.1029/92JD00255.
88. Monteith, J.L.; Unsworth, M.H. *Principles of Environmental Physics: Plants, Animals, and the Atmosphere*, 4th ed.; Elsevier/Academic Press: Amsterdam, The Netherlands; Boston, MA, USA, 2013; ISBN 978-0-12-386910-4.
89. Kustas, W.P.; Norman, J.M. Use of Remote Sensing for Evapotranspiration Monitoring over Land Surfaces. *Hydrol. Sci. J.* **1996**, *41*, 495–516, doi:10.1080/02626669609491522.
90. Sugita, M.; Brutsaert, W. Daily Evaporation over a Region from Lower Boundary Layer Profiles Measured with Radiosondes. *Water Resour. Res.* **1991**, *27*, 747–752, doi:10.1029/90WR02706.
91. Kustas, W.P.; Norman, J.M.; Schmugge, T.J.; Anderson, M.C. Mapping surface energy fluxes with radiometric temperature. In *Thermal Remote Sensing in Land Surface Processes*; CRC Press: Boca Raton, FL, USA, 2004; Volume 2004, pp. 205–253.
92. Kustas, W.P.; Norman, J.M. Evaluation of Soil and Vegetation Heat Flux Predictions Using a Simple Two-Source Model with Radiometric Temperatures for Partial Canopy Cover. *Agric. For. Meteorol.* **1999**, *94*, 13–29, doi:10.1016/S0168-1923(99)00005-2.
93. Li, F.; Kustas, W.P.; Prueger, J.H.; Neale, C.M.U.; Jackson, T.J. Utility of Remote Sensing–Based Two-Source Energy Balance Model under Low- and High-Vegetation Cover Conditions. *J. Hydrometeorol.* **2005**, *6*, 878–891, doi:10.1175/JHM464.1.
94. Otkin, J.A.; Anderson, M.C.; Mecikalski, J.R.; Diak, G.R. Validation of GOES-Based Insolation Estimates Using Data from the U.S. Climate Reference Network. *J. Hydrometeorol.* **2005**, *6*, 460–475, doi:10.1175/JHM440.1.
95. Cristóbal, J.; Anderson, M.C. Validation of a Meteosat Second Generation Solar Radiation Dataset over the Northeastern Iberian Peninsula. *Hydrol. Earth Syst. Sci.* **2013**, *17*, 163–175, doi:10.5194/hess-17-163-2013.